A radiative transfer model for hydrogen recombination line masers

A Prozesky[1] and D P Smits[1]

[1] Department of Mathematical Sciences, University of South Africa, Private Bag X6, Florida 1709, South Africa

E-mail: `prozea@unisa.ac.za`

Abstract. Maser emission arises when spectral lines are enhanced through radiative transfer effects and are observed to be very bright. Molecular astronomical masers have proved to be a very useful tool to probe conditions in a wide variety of sources. Masers are also produced by atomic hydrogen formed by recombination in sufficiently dense HII regions. These hydrogen recombination line (HRL) masers have been observed in a handful of objects to date but the analysis of the atomic physics involved has been rudimentary. In this work a new model of HRL masers is presented that uses an nl-method model to describe the atomic populations interacting with free-free radiation from the plasma, and an escape probability framework to deal with radiative transfer effects. The model is used to describe the general behaviour of radiative transfer of HRLs and to investigate the conditions under which HRL masers form.

1. Background

1.1. Hydrogen recombination line masers

Astronomical masers occur when spectral lines are amplified through stimulated emissions over long path lengths, producing line emission that is much brighter than expected under local thermodynamic equilibrium (LTE) conditions. Traditional astronomical masers occur due to rotational or vibrational transitions of various molecules, and have been studied extensively both observationally and theoretically. More recently, recombination line masers from atomic hydrogen have been observed in a few objects.

[1] showed that recombination lines can be amplified by stimulated emission in the Rayleigh-Jeans limit, even at low optical depths. The theoretical possibility of HRL masers was considered by [2] to account for the anomalous hydrogen line intensities found in dense gasses associated with active galactic nuclei. The first cosmic high-gain HRL maser was discovered in the young stellar object MWC 349A [3, 4]. This maser source has since been studied extensively [5, 6, 7, 8, 9, 10, 11] with the evidence confirming the presence of strongly masing recombination lines. For some time, MWC 349A was the only source in which HRL masers had been detected, but growing interest in the subject has prompted more searches, leading to the identification of a number of HRL masers in other objects, see for example [12], [13], [14] and [15].

The environments in which these atomic masers can form are distinctly different from those of their molecular counterparts. For recombination lines to form, the emitting gas has to be ionized, which for hydrogen requires a temperature of $\sim 10^4$ K. The host clouds of molecular masers are necessarily cooler than the molecules' dissociation temperature and, therefore, are relatively cool ($T \leq 10^3$ K).

A population inversion occurs in hydrogen over a large range of atomic levels in a recombination nebula, whereas in molecular masers the inversion is often limited to a few levels only. A result of this is that many adjacent HRL lines will exhibit masing behaviour at the same time instead of just a few specific lines, as is the case with molecules. In HRL masers, the pumping scheme for the population inversions is a natural consequence of the capture-cascade processes in the atomic component of the ionized gas, which is discussed in more detail in [16]. In many molecular masers the details associated with the pumping scheme are unclear. It should also be noted that because hydrogen makes up the bulk of almost all astronomical gasses, the hydrogen masing lines can be seen in very high column densities. For molecular masers the relevant constituents have low number densities compared to the H_2 content.

There have been some endeavours to construct a theoretical framework for HRL masers. [17] extended the departure coefficient calculations of [18] to higher densities in response to the discovery of the first HRL maser source. [16] addressed the theoretical foundations of HRL masers and considered conditions necessary for their formation.

Most theoretical models for HRL masers have focused on the morphology of the emitting region [8, 19, 11], leading to the suggestion that the masing is strongly related to the structure and kinematics of the emitting gas [20]. Most notable is the three-dimensional non-LTE radiative transfer code MORELI [21]. MORELI uses pre-calculated departure coefficients of either [17] or [22], but does not solve the statistical balance equations (SBE) in a self-consistent way.

[23] incorporated radiative transfer effects into a capture-collision-cascade (C^3) model to assess the effects of saturation on the level populations. They employed an n-model which neglects the effects of the elastic collisions between angular momentum states, as opposed to an nl-model in which they are included. [23] found that the effects of the radiative transfer on the level populations of hydrogen are important.

2. Radiative transfer

The equation of radiative transfer (ERT) describes the radiation added to and subtracted from a given ray as it travels through a medium and is given by

$$\frac{\mathrm{d}I_\nu}{\mathrm{d}l} = -\kappa_\nu I_\nu + j_\nu, \tag{1}$$

where I_ν is the specific intensity and l is the path along the ray. The volume emission and absorption coefficients at the frequency ν are given by j_ν and κ_ν, respectively. The source function is defined as $S_\nu = j_\nu/\kappa_\nu$.

The line emission coefficient j_{nm} describes radiation added to the spectral line of the $n \to m$ transition due to spontaneous emissions and is given by

$$j_{nm} = \frac{h\nu}{4\pi} \sum_{l=0}^{n-1} \sum_{l'=l\pm1} b_{nl} N_{nl}^* A_{nl,ml'} \tag{2}$$

where h is Planck's constant, b_{nl} is the departure coefficient of level nl, N_{nl}^* is the population of level nl in LTE and $A_{nl,ml'}$ is the Einstein A-value for the $nl \to ml'$ transition.

The line absorption coefficient κ_{mn} gives the contribution of absorptions (B_{mn}) and stimulated emissions (B_{nm}) to the emerging radiation field as

$$\kappa_{mn} = \frac{h\nu}{4\pi} \left(N_m B_{mn} - N_n B_{nm}\right) \tag{3}$$

$$= \frac{h\nu}{4\pi} \sum_{l=0}^{n-1} \sum_{l'=l\pm1} b_{ml'} N_{ml'}^* B_{ml',nl} \left(1 - \frac{b_{nl}}{b_{ml'}} e^{-h\nu/kT_e}\right), \tag{4}$$

where k is the Boltzmann constant and T_{e} is the temperature of the free electron gas, which is assumed to have a Maxwellian distribution.

From the definition in equation (3), it is clear that κ_{mn} can become negative if the number of stimulated emissions exceeds the number of absorptions, thereby increasing the line intensity. The term inside brackets in equation (4) is the correction for stimulated emission.

At low enough frequencies, when the continuum is significant, which usually occurs in the Rayleigh-Jeans limit, the line and continuum radiation are formed together. This means the net quantities (indicated by subscripts ν) in equation (1) must take into account the contributions of both the line radiation and the continuum (indicated by subscripts c), so that

$$\kappa_\nu = \kappa_{mn}\phi_\nu + \kappa_{\mathrm{c}}, \qquad j_\nu = j_{nm}\phi_\nu + j_{\mathrm{c}}. \tag{5}$$

where the spectral line shape, assumed to be the same for emission and absorption, is described by ϕ_ν. A box profile with the same line centre maximum as the Doppler profile is assumed for all lines in this work.

The net source function S_ν is given by

$$S_\nu = \frac{j_{nm}\phi_\nu + j_{\mathrm{c}}}{\kappa_{mn}\phi_\nu + \kappa_{\mathrm{c}}}. \tag{6}$$

For an homogeneous medium of thickness L the optical depth is given by

$$\tau_\nu = -L\kappa_\nu. \tag{7}$$

In our models, the continuum absorption coefficient κ_{c} in the Rayleigh-Jeans regime is calculated using the expression of [24]. The continuum emission coefficient is given by $j_{\mathrm{c}} = \kappa_{\mathrm{c}} B_\nu(T_{\mathrm{e}})$, where B_ν is the Planck distribution function.

3. The escape probability approach

When solving a C^3-type model, such as described in [25], it is standard practice to use the Case A/B assumption of [26]. This assumption has been found to work well for nebular conditions where densities are low and line radiation is optically thin ($\tau \ll 1$) [27]. In the other extreme, the cloud is completely optically thick to all line radiation ($\tau_\nu \gg 1$), so that all the level populations have Boltzmann distributions and the mean intensity $J_\nu = B_\nu$.

The escape probability approximation (EPA) addresses the situation between these two extremes: a portion of the radiation is trapped in the cloud and the rest is allowed to escape. If the fraction of photons with frequency ν that escape the cloud is labeled β_ν, then the mean intensity can be approximated by

$$J_\nu = (1 - \beta_\nu) S_\nu. \tag{8}$$

Strictly speaking, β_ν depends on the full solution of the ERT and cannot be calculated locally. However, if an approximation can be derived that depends only on the geometry and local properties of the cloud and is independent of intensity, then the original problem is greatly simplified.

The EPA has been used extensively to model molecular masers (see for example [28, 29, 30, 31, 32, 33]). In this work

$$\beta_\nu = \mathrm{e}^{-\tau_\nu} \tag{9}$$

is used for the escape probability. This form of β_ν does not make any additional assumptions regarding the geometry or the changes in transfer effects throughout the line profile and, therefore, is appropriate to use if these details are not known.

4. The model

The EPA model used here is similar to that of [23] with some important improvements. Most significantly, it includes the effects of the elastic collisions so the calculations are done with a full nl-model. Also, the effects of free-free radiation on the level populations have been incorporated. Nevertheless, we use the same form of the escape probability and general calculational approach.

Our atomic model is based on the C^3 nl-model described in [25] that was adapted to incorporate radiative transfer using the EPA as described in section 3. All atomic rates are as described in [25].

The SBE are solved in the optically thin case ($\beta_\nu = 1$ for all lines) to yield departure coefficients that are equivalent to the ones given in [25] for Case A. From the calculated values of b_{nl}, the net absorption coefficients, emission coefficients and source functions are calculated for each line using equations (2), (4) and (6).

The path length L is then increased and the optical depths and escape probabilities are calculated from equations (7) and (9), respectively. The resulting mean intensities are calculated for each line frequency using equation (8). The SBE are solved again with these values of J_ν incorporated into the rates of the absorption and stimulated processes. The process is repeated for increasing increasing values of L.

values of L.

5. Results and discussion

5.1. Conditions for H masers

The pumping mechanism for hydrogen masers is the ionization-recombination cycle, so it is important that the gas is ionized. Canonically, ionized hydrogen nebulae are taken at $T_e \sim 10^4$, but mechanisms such as forbidden line emission due to high metallicity can cool the gas to much lower temperatures than this while keeping the hydrogen mostly ionized, which occurs in some nova shells. If the electron temperature is too high, the interactions between the free and bound electrons become very fast and the populations of the bound electrons thermalize.

Spectral lines will exhibit high gain maser action if the conditions are such that stimulated emissions become the dominant atomic process and $\tau_\nu < -1$. This requires large column densities along the lines of sight, which can be achieved with either high number densities of hydrogen atoms or long path lengths. Masers require velocity coherence along the amplification path, so there is an upper limit on the path length. The model results show that a path length of $L \sim 10^{16}$ cm is required to have maser action at a density of 10^6 cm^{-3}. Each order of magnitude decrease in N_e results in about an order of magnitude increase required in L to produce the same amplification.


5.2. General trends

Fig. 1 shows how the intensities change as the path length is increased in the model at frequencies of various H$n\alpha$ transitions. For small path lengths, the intensities at all frequencies increase linearly with path length, as is expected for optically thin lines. The behaviour of the line intensities change at the point when $|\tau_\nu| > 1$ in one of two ways, depending on whether τ_ν is positive or negative.

For the conditions shown in Fig. 1, the lines with $n \geq 40$ have positive optical depths. The level populations for these lines are not strictly inverted, but are "overheated" as discussed in [16]. The upper level of these lines are overpopulated with respect to the LTE populations so that the lines are enhanced by stimulated emissions even though the absorption coefficients for these lines are positive. These intensities increase linearly with path length until the cloud becomes larger than their characteristic path length (for which $\tau_\nu = 1$). Once they are optically thick, their intensities remain constant as the size of the cloud is increased, because they cannot be observed from deeper in the cloud than their characteristic path length. The lower frequency

(higher n) lines become optically thick first as L is increased, since the absorption coefficients increase with n beyond the masing lines.

The optical depths of the H15α and H20α lines are negative and their intensities start to increase exponentially with path length when $\tau_\nu < -1$ and maser action sets in. The optical depth of the H5α line is also negative, but $\tau_\nu > -1$ at the path length where the model is terminated.
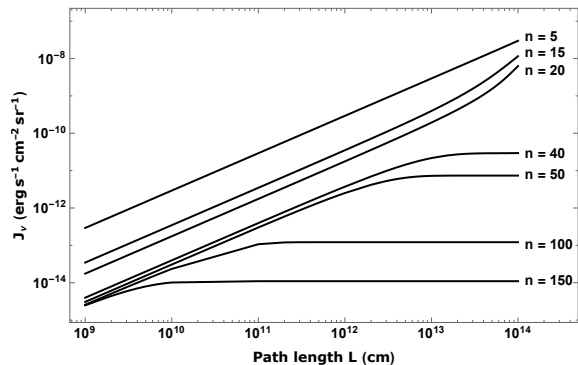
Figure 1. The change of the intensities at frequencies of various H$n\alpha$ transitions with path length for a gas at $T_{\mathrm{e}} = 10^4\,\mathrm{K}$ and $N_{\mathrm{e}} = 10^8\,\mathrm{cm}^{-3}$.
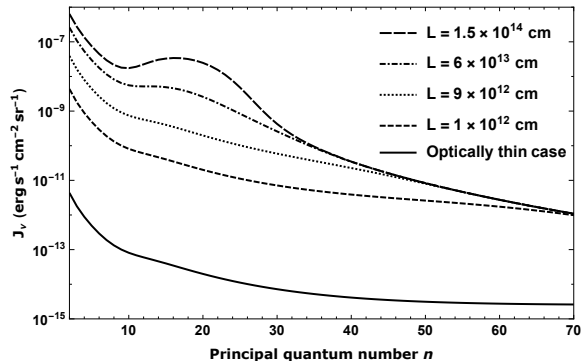
Figure 2. Intensities at the frequencies of H$n\alpha$ transitions with respect to principal quantum number for a gas with $T_{\mathrm{e}} = 10^4\,\mathrm{K}$ and $N_{\mathrm{e}} = 10^8\,\mathrm{cm}^{-3}$ for different path lengths.

Fig. 2 shows the intensities at H$n\alpha$ line frequencies for a gas with $T_{\mathrm{e}} = 10^4\,\mathrm{K}$ and $N_{\mathrm{e}} = 10^8\,\mathrm{cm}^{-3}$ as a function of n for different path lengths. The intensities increase universally from the optically thin values as L is increased as was also illustrated in Fig. 1. As L increases, the lines become optically thick from high values of n, and then do not increase further. If the path length becomes large enough that $\tau_\nu < -1$ for some lines, a bump starts to appear, indicating maser action in the affected lines. As the path length is increased further, the intensities of the masing lines increase significantly with L as the degree of saturation for the masing lines increases.

6. Conclusions

Hydrogen recombination masers are a relatively new field of study with only a small number of examples detected so far. There are some important differences between molecular and atomic hydrogen masers, both on the macro scale, such as in the environments where they form, and at the atomic level, such as in the pumping mechanism and the mutual interaction of many masing lines. The theoretical framework for these objects is still developing and the aim of this paper is to contribute to our understanding by constructing a theoretical model that specifically focuses on the atomic process rather than the geometry and kinematics.

The modeling of masers has some inherent complexities, due to having to solve simultaneously both the local level populations of the masing species, and the non-local radiative transfer of the line photons. Simplifying assumptions, such as the EPA used here, are often employed to make the solutions tractable.

A model for hydrogen recombination masers using the EPA has been constructed to evaluate the general behaviour of hydrogen emission from clouds with conditions where masing is possible. The model results correspond well to our current understanding of how masers grow with increasing path length.

References

[1] Goldberg L 1966 *ApJ* **144** 1225–1231
[2] Krolik J H and McKee C F 1978 *ApJS* **37** 459–483
[3] Martin-Pintado J, Bachiller R, Thum C and Walmsley M 1989 *A&A* **215** L13–L16
[4] Martin-Pintado J, Thum C and Bachiller R 1989 *A&A* **222** L9–L11
[5] Planesas P, Martin-Pintado J and Serabyn E 1992 *ApJ* **386** L23
[6] Thum C, Martin-Pintado J and Bachiller R 1992 *A&A* **256** 507–518
[7] Martin-Pintado J, Neri R, Thum C, Planesas P and Bachiller R 1994 *A&A* **286** 890–897
[8] Ponomarev V O, Smith H A and Strelnitski V S 1994 *ApJ* **424** 976–982
[9] Thum C, Martin-Pintado J, Quirrenbach A and Matthews H E 1998 *A&A* **333** L63–L66
[10] Gordon M A, Holder B P, Jisonna Jr L J, Jorgenson R A and Strelnitski V S 2001 *ApJ* **559** 402–418
[11] Weintroub J, Moran J M, Wilner D J, Young K, Rao R and Shinnaga H 2008 *ApJ* **677** 1140–1150 (*Preprint* `0801.0608`)
[12] Cox P, Martin-Pintado J, Bachiller R, Bronfman L, Cernicharo J, Nyman L A and Roelfsema P R 1995 *A&A* **295** L39–L42
[13] Jiménez-Serra I, Báez-Rubio A, Rivilla V M, Martín-Pintado J, Zhang Q, Dierickx M and Patel N 2013 *ApJ* **764** L4 (*Preprint* `1212.0792`)
[14] Aleman I, Exter K, Ueta T, Walton S, Tielens A G G M, Zijlstra A, Montez R, Abraham Z, Otsuka M, Beaklini P P B, van Hoof P A M, Villaver E, Leal-Ferreira M L, Mendoza E and Lépine J D R 2018 *MNRAS* **477** 4499–4510 (*Preprint* `1805.06496`)
[15] Murchikova E M, Phinney E S, Pancoast A and Blandford R D 2019 **570** 83–86 (*Preprint* `1906.08289`)
[16] Strelnitski V S, Ponomarev V O and Smith H A 1996 *ApJ* **470** 1118–+ (*Preprint* `arXiv:astro-ph/9511118`)
[17] Walmsley C M 1990 *A&AS* **82** 201–206
[18] Brocklehurst M and Salem M 1977 *Computer Physics Communications* **13** 39–48
[19] Strelnitski V S, Smith H A and Ponomarev V O 1996 *ApJ* **470** 1134 (*Preprint* `astro-ph/9511119`)
[20] Martín-Pintado J 2002 *Cosmic Masers: From Proto-Stars to Black Holes* (*IAU Symposium* vol 206) ed Migenes V and Reid M J p 226
[21] Báez-Rubio A, Martín-Pintado J, Thum C and Planesas P 2013 *A&A* **553** A45 (*Preprint* `1307.3896`)
[22] Storey P J and Hummer D G 1995 *MNRAS* **272** 41–48
[23] Hengel C and Kegel W H 2000 *A&A* **361** 1169–1177
[24] Oster L 1961 *Rev. Mod. Phys.* **33** 525–543
[25] Prozesky A and Smits D P 2018 *MNRAS* **478** 2766–2776 (*Preprint* `1805.02440`)
[26] Baker J G and Menzel D H 1938 *ApJ* **88** 52
[27] Osterbrock D E 1962 *ApJ* **135** 195–+
[28] Sobolev A M, Cragg D M and Godfrey P D 1997 *A&A* **324** 211–220
[29] Cragg D M, Sobolev A M and Godfrey P D 2002 *MNRAS* **331** 521–536
[30] Langer S H and Watson W D 1984 *ApJ* **284** 751–768
[31] Chandra S, Kegel W H, Albrecht M A and Varshalovich D A 1984 *A&A* **140** 295–302
[32] Röllig M, Kegel W H, Mauersberger R and Doerr C 1999 *A&A* **343** 939–942
[33] Humphreys E M L, Yates J A, Gray M D, Field D and Bowen G H 2001 *A&A* **379** 501–514